A computational method for segmenting topological pointsets and application to image analysis

A Computational Method for Segmenting Topological Point-Sets and Application to Image Analysis

Stiliyan N. Kalitzin, Joes Staal, Bart M. ter Haar Romeny, *Senior Member*, *IEEE*, and Max A. Viergever

Abstract—We propose a new computational method for segmenting topological subdimensional point-sets in scalar images of arbitrary spatial dimensions. The technique is based on calculating the homotopy class defined by the gradient vector in a subdimensional neighborhood around every image point. This neighborhood is defined as the linear envelope spawned over a given subdimensional vector frame. In the simplest case where the rank of this frame is maximal, we obtain a technique for localizing the critical points, i.e., extrema and saddle points. We consider, in particular, the important case of frames formed by an arbitrary number of the first largest by absolute value principal directions of the Hessian. The method then segments positive and and negative ridges as well as other types of critical surfaces of different dimensionalities. The signs of the eigenvalues associated to the principal directions provide a natural labeling of the critical subsets. The result, in general, is a constructive definition of a hierarchy of point-sets of different dimensionalities linked by inclusion relations. Because of its explicit computational nature, the method gives a fast way to segment height ridges or edges in different applications. The defined topological point-sets are connected manifolds and, therefore, our method provides a tool for geometrical grouping using only local measurements. We have demonstrated the grouping properties of our construction by presenting two different cases where an extra image coordinate is introduced. In one of the examples, we considered the image analysis in the framework of the linear scale-space concept, where the topological properties are gradually simplified through the scale parameter. This scale parameter can be taken as an additional coordinate. In the second example, a local orientation parameter was used for grouping and segmenting elongated structures.

Index Terms—Differential topology, critical point-sets, ridges, image analysis, scale space.

1 Introduction and Related Works

In this paper, we introduce a topological quantity that characterizes the neighborhood of every pixel in scalar images of arbitrary spatial dimensions. This quantity is an integer number that can single out critical points such as extrema and saddle points. It can also be generalized to define the membership of the point to extended subdimensional structures such as ridges or edges. The topological homotopy class number was introduced in [7], [8], [9] in relation to its importance for the deep-structure image analysis and application to multiscale segmentation. In its essence, this number reflects the behavior of the gradient image vector in a close neighborhood around the given test point. In the simplest one-dimensional case, the topological class of a point is defined as the difference of the sign of the signal derivative taken from both sides of the point. Clearly, this number is zero everywhere except in the local extrema.

The proper generalization to higher dimensions is provided by the homotopy class $\pi_{D-1}(S^{D-1})$ that parameterizes the space of nonequivalent (nondeformable smoothly into each other) mappings between two $D-1$ dimensional spheres (D is the number of dimensions of the image). The mapping is defined by the normalized gradient vector taken on a closed surface (homotopic to a sphere) surrounding the test point. One can show that the set of nonequivalent mappings for $D>1$ can be labeled with an integer number. This is particularly evident in the $D=2$ example, where the topological number reduces to the well-known winding number [10], indicating the number of times the gradient vector rotates around its origin when a point is circumventing the test point. Extrema points have winding number $+1$, saddle points are with winding number -1, and, for regular points, the number vanishes. A detailed discussion on the 2D case is presented in [7] and, in the next section, we give a concise summary of the construction as well as of its generalization to arbitrary image dimensions.

The main advantage of using homotopy classes for localizing singular points lies in their explicit and constructive nature. In finding the zero crossings of a real function, for example, the only sensible task would be to find the intervals where the function changes sign. The size of these intervals is the precision with which we are searching for the zero crossings. Our topological construction is, in many aspects, analogous to this generic example. The size of the neighborhood (the closed surface) around the test image point is the spatial precision with which we want to localize the singular point. Therefore, our method is

- *S.N. Kalitzin is with the Dutch Epilepsy Clinics Foundation, Achterweg 5, 2103 SW Hemmstede, The Netherlands. E-mail: skalitzin@sein.nl.*
- *J. Staal, B.M. ter Haar Romeny, and M.A. Viergever are with the Image Science Institute, Utrecht University, University Medical Center, E01.334, Heidelberglaan 100, 3584 CX Utrecht, The Netherlands. E-mail: {joes, bart, max}@isi.uu.nl.*

Manuscript received 8 Jan. 1999; revised 28 July 1999; accepted 14 Aug. 2000. Recommended for acceptance by I. Sethi.
For information on obtaining reprints of this article, please send e-mail to: tpami@computer.org, and reference IEEECS Log Number 108934.

a natural generalization of interval calculus to higher dimensional signals.

Another advantage of the proposed quantity is its nonperturbative nature. To compute the homotopy class of a point, we do not need to know the values of any set of derivatives *in* the point. We only sum certain quantities (differential forms) *around* the given image location. The quantity is *additive*, so the total topological number surrounded by a given surface is the sum of the topological number of all image points inside. This feature enables the selection of the neighborhood size as the singularity resolution parameter and makes the whole construction well-posed.

In addition to segmentation of critical points, the method is extended in this paper for localization of points lying on *relative critical sets*. To this end, we introduce a *relative homotopy class* of a given test image point defined as the homotopy class calculated on a linear subspace in the neighborhood of the test point. This subspace can be defined as a linear envelope spawned over the vectors of a given vector frame field. A particularly important case is that of the frame formed by a subset of the eigenvectors of the Hessian (the matrices of the second image derivatives). In this case, we obtain a constructive definition for *topological ridges*. We can classify such a point-set by the number of the Hessian eigenvectors forming the subspace and by the signs of the corresponding eigenvalues. We show in the paper that our definition is equivalent in some particular cases to the definitions given in [2], [3], [4], [11], [15]. In the last works, the point-sets are defined implicitly and, here, we propose a direct computational technique that segments the point-sets explicitly. In addition to ridges, we can define other particular relative critical sets by using any globally biased frame field where a number of vectors are chosen independently of the image structures.

Another interesting case is the hyperdimensional critical set defined relative to the gradient vector itself and segmented by the zero-crossings of the second derivative in the direction of the gradient. This point-set can be interpreted as a *topological edge*.

Critical points and ridges play an essential role in uncommitted image analysis, as revealed in [12], [13]. Similar topological structures were studied in the context of multiscale image analysis [6], [14], [16], [18]. They form a sort of a topological back-bone on which the image structures are mounted. One specific feature of our construction is that it relies on quasi-local image properties. This distinguishes it from the watershed model [18].

The rest of the paper is organized as follows:

In Section 2, we remind the reader of the basic definitions and properties of the topological feature introduced in [7], [8] that enable localizing singular points in gray-scale images. Section 3 extends the latter definitions to the concept of critical point-sets of higher subdimension. We introduce a classification of these critical sets that can be relevant for image analysis. In particular, we define relative critical point-sets defined by the local Hessian. These point-sets can be interpreted as topological ridges of various signature. Further, we consider another class of critical point-sets that can be interpreted as topological edges. In Section 4, we present some examples in various image dimensions. The technique is applied either to the original image or to an expanded data-space built over the image. We consider the case of a scale space image representation and the case of an orientation space representation. We show that our method further provides a tool for structural *grouping* when applied to expanded image representations. Section 5 compares our results with those obtained from an alternative definition for ridges. We summarize in this section the applicability of the method, possibly in conjunction with other techniques, to segmentation tasks in image processing. The main conclusions of this work are summarized in Section 6. Finally, our discrete implementation of the method is outlined in the Appendix.

2 Homotopy Numbers

We start this section with two simple and intuitive examples—the set of critical points in one- and two-dimensional signals (images). The purpose of these examples is to provide an inductive basis for generalizations in images of arbitrary dimension.

A critical point of a D-dimensional image $L(x_1, \ldots, X_D)$ is a point where the gradient vector $\partial_i L(x_1, \ldots, X_D), i = 1, \ldots, D$ vanishes. In the one-dimensional case, this is a point where the first derivative makes a zero crossing. To localize such a point, it is enough to consider, in the one-dimensional case, the difference $\nu_P \equiv \mathrm{sign}(\partial_x L)_B - \mathrm{sign}(\partial_x L)_A$ for any A, B: $A < P < B$ in the close vicinity of a test point P. Obviously, the zero crossings of the signal derivative are the points where the latter changes its sign and, therefore, can be characterized with the condition $\nu_P \neq 0$. Moreover, because in 1D-signals critical points are either minima or maxima, $\nu_P = 2$ indicates that in the neighborhood of P lies a minimum and $\nu_P = -2$ indicates that in the neighborhood of P lies a maximum of the signal. The size of the interval $[A, B]$ defines the *precision* with which we want to localize the critical point. If we consider the above quantity $\nu(x)$ for all signal points x, then we will obtain, roughly speaking, the distribution of the critical points for the whole signal.

The same procedure is far less trivial in the case of a two-dimensional image $L(x, y)$. To localize the spatial locations where the image gradient $\partial_x L, \partial_y L$ vanishes, we can consider the *winding number* [10]:

$$\nu_P = \oint_C (L_x dL_y - L_y dL_x), \tag{1}$$

where the integral is taken along a closed curve surrounding the test point P. The expression in the integral in (1) is the infinitesimal angle of rotation of the gradient vector as the integration goes along the curve C. It is not difficult to see that, if the contour C encompasses an extrema point (minimum or maximum), the quantity (7) takes value $+2\pi$. If a saddle point is enclosed by C, then $\nu_P = -2\pi$. These two cases are illustrated in Fig. 1.

In degenerate saddle points, also called "monkey saddles," the topological number is $-2(n-1)\pi$, where n is the number of ridges or valleys converging to the point.

In the same way as in the one-dimensional case, by computing the quantity (1) for all image points, we can

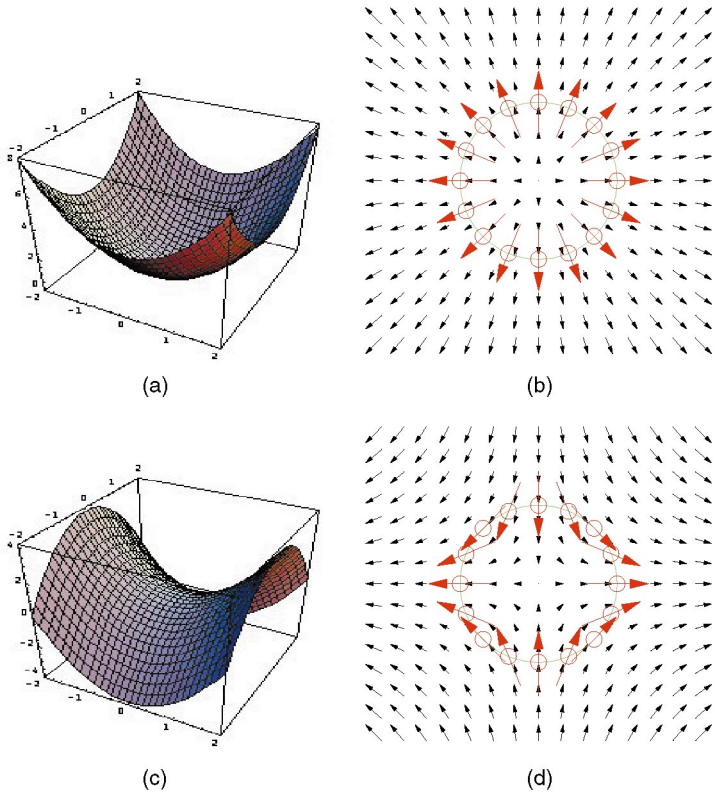

Fig. 1. (a) Graph of a synthetic 2D image with minimum in $(0,0)$ described analytically as $L(x,y) = x^2 + y^2$. (b) The gradient vector field is represented as a lattice of small black arrows, the integration contour C is the green circle, and, at the 16 running integration positions (red circles), the gradient vector is represented as a red arrow. It makes a 2π rotation around the contour. (c) Graph of a synthetic image with a saddle point in $(0,0)$ described analytically as $L(x,y) = x^2 - y^2$. (d) The same as in (b) but for the saddle point image. The gradient vector returns in its original position after a -2π turn.

obtain another image containing information about the positions and the type of the critical points in the original gray-scale image. The spatial precision in this case is determined by the size of the area surrounded by the contour C.

Formula (1) is the starting point for higher dimensional extension of the concept of winding number. In [7], we give self-contained definitions of our quantities as well as a detailed proof of their essential properties. Here, we present the highlights of the construction and introduce some brief notations from the theory of homotopy groups [17] that provide the natural basis for the introduction of a topological number associated to any singular image point.

Suppose P is a point in the image (singular or regular) and V_P is a region around P which does not contain any singularities except possibly P. Now, we will define a quantity characterizing the image in the surrounding of the point P. Let S_P be a closed hypersurface, topologically equivalent to a $D-1$-dimensional sphere such that it is entirely in V_P and our test point P is inside the region W_P bounded by S_P. In other words,

$$P \in W_P : S_P = \partial W_P. \tag{2}$$

Because, by assumption, there are no singularities in $S_P \in V_P$, the normalized gradient vector field

$$\xi_i = \frac{\partial_i L}{\sum_j (\partial_j L \partial_j L)^{1/2}}, \tag{3}$$

$$L_i \equiv \partial_i L, \tag{4}$$

is well-defined on the surface S_P.

The space of all unit-length D-dimensional Euclidean vectors is isomorphic to the $D-1$-dimensional sphere of unit radius $S_1^{(D-1)}$. Therefore, the vector field ξ_i defines a mapping

$$S_P \to S_1^{(D-1)}.$$

But, recalling that S_P is a manifold homotopic to a $D-1$-dimensional sphere, we see that the above mapping can be classified by an element of the homotopy group $\pi_{(D-1)}(S^{(D-1)})$. This group comprises all homotopically nonequivalent mappings between two $D-1$-dimensional spheres. It is known that $\pi_{(D-1)}(S_1^{(D-1)}) \equiv \mathbf{Z}$, which is the Abelian group of all integer numbers (where addition is the group operation). We can characterize the vector field ξ_i on the surface S_P taken around the chosen point P by the homotopy number (the element of $\pi_{(D-1)}(S^{(D-1)})$) of the mapping it defines. This number ν is independent of the surface S_P as long as $S_P \in V_P$ since then the surface does not surround singularities other than possibly P. Therefore, the defined local topological number ν characterizes only the image neighborhood of the point P and not the hypersurface on which it is measured.

To make the above ideas computationally explicit, we first give the operational definition of the quantity ν:

Definition 1. *Let $L(x): R^D \to R$ be a differentiable D-dimensional scalar image represented by its **gray-scale function** with at most isolated singularity points. At a **nonsingular** point $A = (x_1, \ldots, x_D)$, we define a $(D-1)$ form:*

$$\begin{aligned}\Phi(A) &= \sum_{i_1 \ldots i_D} L_{i_1} dL_{i_2} \wedge \cdots \wedge dL_{i_D} \epsilon^{i_1 i_2 \ldots i_D} \\ &\equiv \sum_{i_1 \ldots i_D} \xi_{i_1} d\xi_{i_2} \wedge \cdots \wedge d\xi_{i_D} \epsilon^{i_1 i_2 \ldots i_D}\end{aligned} \tag{5}$$

$$\epsilon^{i_1 i_2 \ldots i_k \ldots i_l \ldots i_D} = -\epsilon^{i_1 i_2 \ldots i_l \ldots i_k \ldots i_D} \text{ for any } l \neq k; \epsilon^{12 \ldots D} = 1. \tag{6}$$

Definition 2. *With the same conditions as in Definition 1, let S be a closed $(\partial S = 0)$, oriented hypersurface. If there are no singularities on S, then we define the quantity:*

$$\nu_S = \oint_{A \in S} \Phi(A). \tag{7}$$

The integral above is the natural integral of a $(D-1)$ form over a $(D-1)$-dimensional manifold without border.

An important property of the $(D-1)$ form Φ is that it is a closed form or:

Proposition 1.

$$d\Phi(A) = 0. \tag{8}$$

The above property of the form (5) is essential for the applications of the topological quantity (7). If W is a region where the image has no singularities, then the form Φ is defined for the entire region W and we can apply the generalized Stokes theorem [1], [5]:

$$\oint_{\partial W} \Phi^{(D-1)} = \int_W d\Phi^{(D-1)} \equiv 0, \tag{9}$$

because of (8). Therefore, we obtain

Corollary 1. *If the gray-scale function $L(x)$ has no singularities in a given region W, then the topological quantity (7) is identically zero.*

Consider now a smooth local deformation of the surface S. If no singularities are crossed by S in the process of this deformation, then the region swept by the surface will be free of singularities and, therefore, the topological number on its border is zero. But, the border of this region is composed exactly of the initial surface, with its orientation inverted, and the deformed surface. It is easy to see that (7) is *additive* or, in other words, $\nu_{S_1 \cup S_2} = \nu_{S_1} + \nu_{S_2}$, where S_1 and S_2 are two hypersurfaces. The integral defining ν_S obviously changes its sign when changing the orientation of the surface of integration. Therefore, the quantity (7) on the initial and the deformed surfaces is equal as their difference is zero. This leads to the property that the topological number (7) is invariant under smooth deformations of the hypersurface S as long as no singularities are crossed by the boundary. The last property justifies the term "topological" that we assign to the quantity ν_S. It depends on the properties of the image in the region where S is placed, but, in general, not on the surface S itself. More precisely, the topological number depends only on the number and type of singularities surrounded by the surface S. From an implementation point of view, the topological nature of the quantity (7) allows the computation to take place on any surface around the test point.

Topological numbers ν_P can be associated with every point of the image if, in (7), S is **any** closed oriented hypersurface taken closely around a test point P. The surface S must be close to P in order to ensure that no other singularities are surrounded. It is clear from Proposition 1 and the integral Stokes' theorem, however, that the topological number of a nonsingular point is zero. If we plot the value of ν_P in every point of an image, we will obtain a map of the singularities of the image representing their topological "charge." We can go one step further and define a *scalar density field*, $\nu(x_1, x_2, \ldots, x_D)$, that gives the *distribution* of the topological singularities in a given image. The point-set is defined as the set of locations (pixels) where $\nu \neq 0$ will give the set of all singular points in the image. Examples for this construction in different spatial dimensions were presented in the beginning of this section and can be found in more detail in [7].

In [8], we present in detail the mechanism of grouping of the singularities in strings when scale evolution is considered. Topological numbers defined with (7) play an essential role in understanding the evolution of singularities across scale. As a consequence of a "conservation law," singularities preserve their topological numbers while drifting across scale as long as they do not come infinitely close to other singularities.

3 Critical Sets Relative to Vector Subframes

3.1 General Construction

In what follows, we extend the definition of a local homotopy number by introducing suitable linear subneighborhoods around every image point. The new idea is to select, at every image point P, a *local linear subspace* K_P and to project the gradient vector $L_i = \partial_i L$ onto it:

$$L_\alpha(x) = \sum_i h^i_\alpha(x) L_i(x). \tag{10}$$

Here, $h^i_\alpha, \alpha = 1, \ldots, D_K$ are the local frame vectors defining the linear subspace K with dimension $D_K < D$.

The next step is to compute the *relative homotopy number* in point $P \in R^D$ in analogy with (7).

Definition 3. *The topological charge in point P relative to the local subframe h_α is*

$$\nu_P(K_P) = \oint_{A \in S_P, S_P \in K_P} \Phi(A), \tag{11}$$

where now the closed surface S_P around P is of dimension $D_K - 1$ and lies in the subspace $K_P \equiv LE(h_\alpha(P))$, where $LE()$ stands for linear envelope. The $(D_K - 1)$ form Φ is computed as in (5), but from the vector field (10).

We assume that the set of vectors $h_\alpha(P), \alpha = 1, \ldots, D_K$ is of maximal rank D_K and, therefore, the local linear space K_P is of dimension D_K.

Now, we define our central construct, the topological critical set, relative to the subframe h.

Definition 4. *Let $h(x)$ be a local nondegenerate subframe of dimension (rank) D_K and let the local linear envelope of this frame be K_x. The point-set*

$$PS(h) : \{x; x \in R^D, \nu_x(K_x) \neq 0\} \tag{112}$$

is the relative critical point-set (RCPS) associated to the local frame h.

From the property of the topological number given in Corollary 1, Definition 4 implies $L_\alpha(P) = 0$ when $P \in PS(h)$. Therefore, our RCPS are equivalent to those defined in [2], [3], [4] for the same frame fields.

It is clear that if $D_K = D$, i.e., if the local subframe is complete, the relative homotopy class (11) is just the full homotopy class. The manifold defined in Definition 4 will then be of dimension 0. In fact, this set is the set of all critical points in the image.

In addition to the feature that the topological number (11) is nonzero, the RCPS can be characterized by the value of this number and, eventually, by some characteristic properties of the subframe h.

Now, we address the question of the *local topological structure* of the RCPS associated with an arbitrary subframe h^i_α. We show in what follows that:

Proposition 2. *If point P belongs to the relative critical point-set from Definition 4 and if the Hessian in P is nonsingular, then the point-set is locally isomorphic to a linear space of dimension $D - D_K$.*

The following proof uses some techniques from differential geometry that provide adequate covariant formalism.

Proof 1. Let the subframe $h^i_\beta, \beta = D - D_K + 1, \ldots, D$ be chosen in such a way that the system of vectors h_α, h_β represents a complete frame in the D-dimensional space of the image and $\sum_I h^i_\alpha h^i_\beta = 0$ for all α, β from the corresponding ranges. If the point P belongs to the RCPS defined by the subframe h_α, then, obviously, $L_\alpha \equiv \sum_i h^i_\alpha \partial_i L(P) = 0$. If P has coordinates x^i, then the infinitesimally close point with coordinates $x^i + \delta x^i$ will belong to the same RCPS if $\sum_A \delta x^A \nabla_A L_\alpha = 0$, where the index A takes all values of $1, \ldots, D$; $\delta x^A \equiv \sum_I (h^{-1})^A_i \delta x^i$ and ∇_A is the *covariant derivative* induced by the frame h_A (such that $\nabla_A h_B = 0$). Applying these notations, we obtain the following equation for the variation δx^i:

$$\sum_{i,j} \delta x^i h^j_\alpha \partial_i \partial_j L(P) = 0. \tag{13}$$

Using the completeness of the system h_A and the orthogonality between h_β and h_α, we obtain:

$$\sum_I \delta x^i \partial_i \partial_j L(P) = \sum_\beta C^\beta h^j_\beta, \tag{14}$$

where C^β are $D - D_K$ arbitrary constants. If the Hessian $H_{ij} \equiv \partial_i \partial_j L(P)$ is nonsingular, it can be inverted giving the following form of the RCPS coordinate variations:

$$\delta x^i = \sum_{i,\beta} (H^{-1})^{ij} h^j_\beta C^\beta. \tag{15}$$

Clearly, the system $g^j_\beta \equiv \sum_j (H^{-1})^{ij} h^j_\beta$ has rank $D - D_K$ as it is obtained by a nonsingular linear transformation from the subframe h_β. Therefore, the variations in (15) belong to the $D - D_K$ dimensional linear envelope over the subframe g_β. □

The above proposition motivates the introduction of RCPS as topological manifolds. It is clear from the proof that these manifolds are continuous for all points where both the image Hessian and the subframe are defined and nonsingular.

In the following section, we give some important examples of RCPS associated with a subset of the principal eigenvectors of the local Hessian.

3.2 Definition and Detection of Topological Ridges

Let the local Hessian field $H_{ij} \equiv \partial_i \partial_j L(x)$ have eigenvalues $\lambda_1, \ldots, \lambda_D$ with corresponding eigenvectors $h_1, \ldots, h_D$. We can assume that the eigenvalues are labeled in decreasing order of their absolute values: $|\lambda_1| > \cdots > |\lambda_D|$. There are different ways to select a subset of eigenvectors to form the subframe h in Definition 4. In what follows, the following definition is most suitable for the interpretation of the RCPS as height ridges and their generalizations.

Definition 5. *A topological ridge set $R^{(m_+, m_-)}(L)$ of co-dimension $m_+ + m_- \equiv D_K$ is defined as an RCPS associated with the Hessian eigenvectors $h_1, \ldots, h_{D_K}$ corresponding to the D_K largest by absolute value of the eigenvalues $\lambda_\alpha, \alpha = 1, \ldots, D_K$. Excluded are points where the Hessian is degenerate so that there is no unique set of λ_α. In the thus defined point-set, only those points are included where there are exactly m_+ positive and m_- negative Hessian eigenvalues.*

This definition puts a natural label on the topological ridge. For example, if $m_+ = 0, D_K = m_-$, we obtain a classical height ridge, if $m_- = 0, D_K = m_+$, we have a valley. In the general cases where $m_+ \neq 0; m_- \neq 0$, we can talk of "saddle ridges." The definition extends the $D_K = D$ case where the ridge is of dimension zero. Then, we have the possibilities of maxima, minima, and saddle points of different signature. Note that the classification implied by Definition 5 is richer than the one induced from the value of the topological number alone. For nondegenerate critical points, the homotopy class is equal to the sign of the determinant of the Hessian (see detailed proof in [8]). Obviously, a lot of different signatures discriminated by Definition 5 will have the same homotopy number.

As a consequence from Proposition 2, the topological ridges are manifolds of dimension $D - D_K$. In this case, the vectors h_α are eigenvectors of the Hessian and we can choose the frame h_α, h_β from Proof 2 to be the entire system of eigenvectors of H_{ij} (and, therefore, also of $(H^{-1})_{ij}$).

In the case of topological ridges, we have $\sum_j H_{ij} h^j_\alpha \equiv \sum_\alpha \lambda_\alpha h^i_\alpha$ for all $\alpha = 1, \ldots, D_K$ and, therefore, (13) takes the form:

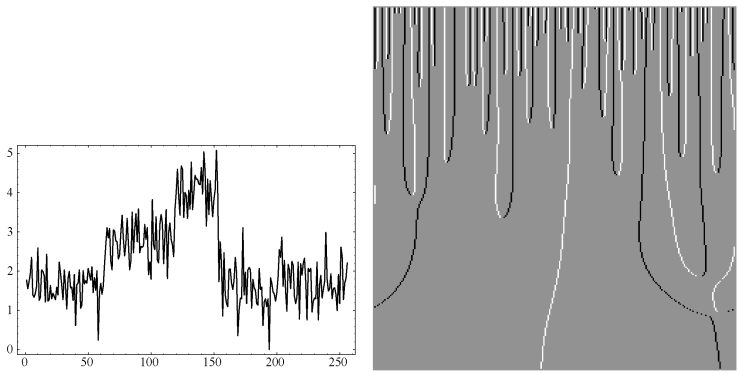

(a) (b)

Fig. 2. (a) One-dimensional signal of 256 data points. (b) Scale space evolution of the one-dimensional topological number. The vertical axis represents the scale parameter. Light and dark lines represent evolution of maxima and minima respectively. Both types of singular points annihilate at catastrophe points.

$$\lambda_\alpha \sum_i \delta x^i h^i_\alpha = 0. \tag{16}$$

It is easy to see that if $\lambda_\alpha \neq 0$ for all α, then (15) now takes the simpler form:

$$\delta x^i = \sum_\beta h^i_\beta C_\beta. \tag{17}$$

Therefore, in addition to general RCPS properties, the topological ridges are locally *orthogonal* to the vector system h_α.

A different definition may include the eigenvectors corresponding to the first D_K eigenvalues of the Hessian ordered by their *signed value*. Such a scheme is extensively studied in [2]. The corresponding classification in that case will partially overlap with ours, namely, for the cases of $R^{m,0}$ and $R^{0,m}$ RCPS (strict positive or strict negative ridges). For the mixed signatures, the two schemes will segment out different topological manifolds. We note that our general constructive approach from Definition 4 can be used for both of the definitions. A comparison of the different vector frame field choices and their relations will appear in a forthcoming publication.

3.3 Inclusion Hierarchy of Ridges

A direct consequence of the definition of topological ridges as relative critical sets is the relation:

$$m^+ \geq m'^+; m^- \geq m'^- \rightarrow R^{(m_+,m_-)}(L) \in R^{(m'_+,m'_-)}(L). \tag{18}$$

The importance of this inclusion is discussed in the next section, where it provides a way for detection of both critical lines and their annihilation points in one-dimensional signals. Another practical application includes detection of the optimal scale for elongated image structures and simultaneously establishing a link to the finest scale.

3.4 Topological Edges

In order to illustrate our geometrical construction, we modify Definition 5 to localize edges or borders between gray-scale objects in images. A trivial approach to this issue would be to define the system of edges as the point-set $R^{0,1}$ taken on the gradient magnitude $|\nabla L(x)|$ of the image $L(x)$. This construction can be useful, but it involves higher order differentials (the Hessian of the gradient will contain third order derivatives of the original image), so we can propose a *second order alternative*.

Definition 6. *A topological edge is the point-set $E(L)$, where the quantity*

$$\eta(x) = \operatorname{sign}\left(\sum_{i,j} \xi^i \xi^j H_{ij}(x + \rho\xi)\right) - \operatorname{sign}\left(\sum_{i,j} \xi^i \xi^j H_{ij}(x - \rho\xi)\right) \tag{19}$$

is equal to -2. Here, H_{ij} is the local Hessian tensor, ξ_i is the normalized gradient vector as in (5), and ρ is a small constant defining the precision with which we want to localize the edge.

In fact, (19) is just the difference in sign of the second derivative in the direction of the gradient. In our notation, we interpret the topological edge as a RCPS defined by the one-dimensional vector frame constituted by the gradient field.

4 Examples of RCPS in Images

Here, we present different instances of the point-sets $R^{m_+,m_-}(L)$ and $E(L)$.

The first example, presented in Fig. 2, illustrates both the concept of the one-dimensional homotopy number and the scale-space evolution properties of the corresponding point-sets (the sets of critical points in this case). All possible cases are summarized in Table 1. The RCPS in this case are discrete point-sets that consist of all maxima $R^{0,1}$ and all minima $R^{1,0}$.

TABLE 1
The Possible Point-Sets for One-Dimensional Signals

m_+ / m_-	0	1
0	regular	minimum
1	maximum	x

An "x" stands for an impossible configuration.

TABLE 2
The Possible Point-Sets for Two-Dimensional Signals

m_- \ m_+	0	1	2
0	regular	negative ridge	minimum
1	positive ridge	saddle	x
2	maximum	x	x

An "x" stands for an impossible configuration.

The second example uses the same input as in Fig. 2 but, instead of tracing the scale-space evolution of the critical points, we regarded the whole scale-space of the original signal as a two-dimensional signal (the second dimension is the scale). We can then localize the ridges $R^{1,0}$, $R^{0,1}$ as well as the 2D critical point-sets $R^{2,0} \cup R^{0,2}$ (this is the set of all extrema) and $R^{1,1}$ (the set of all saddle points). For a listing of all cases, refer to Table 2. We see that the inclusion property (18) assigns the set of saddle points as the set of annihilation points for the 1D critical trajectories in Fig. 2, whereas they appear as 2D positive and negative ridges in Fig. 3. Noticeably, there are no extrema points ($R^{2,0}$ or $R^{0,2}$) in this figure. The reason is that the linear diffusion that generates the scale-space of the signal does not create new minima or maxima beyond the initial scale. This also implies that the linear diffusion does not allow for scale selection.

An example where all relative point-sets are present can be obtained by taking the natural derivatives of the 1D signals and their scale evolution. This means that new maxima and minima can be created beyond the initial scale, allowing for scale selection. We illustrate this with a 1D signal from which we take the natural second derivative across scale and look, as in the previous case, at the two-dimensional critical point-sets of this scaling derivative. Natural derivatives are dimensionless derivatives, which allows for comparing derivatives of different orders, since their dimension is equal. They are defined by multiplying the normal derivative by the scale

$$\overline{\partial}_i = \sigma \partial_i, \tag{20}$$

with $\overline{\partial}_i$ the natural derivative and $\sigma \equiv \sqrt{t}$ the scale.

Fig. 4 shows the point-sets for the second natural derivative of the one-dimensional signal of Fig. 2. We see that the local maxima and minima are subsets of the ridges and valleys, as was stated in (18). Most of the saddle points are annihilation points of the ridges and valleys. Saddle-points on a ridge are local minima in the direction of the ridge, i.e., the direction of the eigenvector of the smallest absolute eigenvalue. On a valley, they are local maxima in that direction.

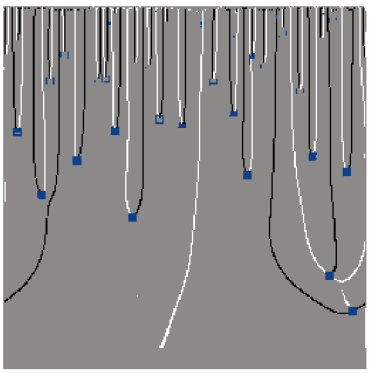

Fig. 3. For the same 1D signal as in Fig. 2a, we first build the scale-space and then localize the ridges (white) and valleys (black) and the singular saddle points (blue).

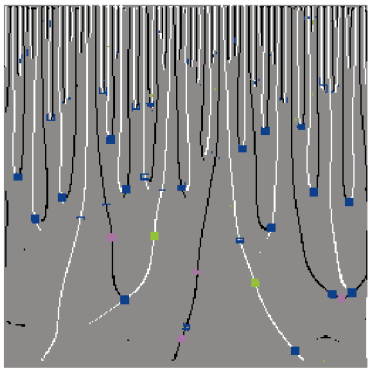

Fig. 4. The topological point-sets for the second natural derivative of the 1D signal of Fig. 2. White corresponds to positive ridges, black to negative ridges, blue to saddle points, green to maxima, and purple to minima.

We see in Fig. 4 that all possible point-sets as classified in Table 2 occur. The local maxima and minima points, $R^{0,2}$ and $R^{2,0}$, serve as scale selectors, the points at which maximum response—in the absolute sense—of the filter is found. These points are an indication of the scale at which structure in the original signal is observed. Via the ridge or valley to which an extremum belongs, we can trace back to the finest scale, which restores the location of the local structure. Since we have taken the second derivative, this will be a needle-like structure. For large scales, the positive and negative ridges annihilate each other in saddle points. These points select the scale up to which structure exists, i.e., up to which scale it can be observed.

In the last two examples, the 2D technique was used in the scale-spaces generated by a one-dimensional signal. The complete relative critical set system of a 2D image is given in Fig. 5. Note the inclusion relations between the different RCPS.

Now, we turn to the 3D case. The possible RCPS are listed in Table 3. Note that, in this case, we have ridges of two different dimensionalities representing correspondingly surfaces and strings. The saddle points are also of two possible types: $R^{2,1}$ and $R^{1,2}$.

As an example of the topological method in 3D, we analyze the 3D scale-space built over a two-dimensional image of an anisotropic Gaussian blob with $\sigma_x = 5.0$ and $\sigma_y = 35.0$ pixels, see Fig. 6a. We computed the scale space of this image, i.e., we blurred it with a two-dimensional Gaussian filter, for 64 scales, running exponentially from 1.0 to 20.0 pixels. The only critical sets we can find from the scale space are surfaces and strings. Local extrema ($R^{0,3}$ and $R^{3,0}$) cannot be found, as was the case in the two-dimensional scale space example (Fig. 3), because of the attenuation of the diffusion equation. In Fig. 6b, we show, in blue, the positive surface of the scale space of Fig. 6a and, in green, the string of maxima. These are the only critical subsets that can be found for this image. Note that, on a fixed scale, the positive surface is nothing more than the

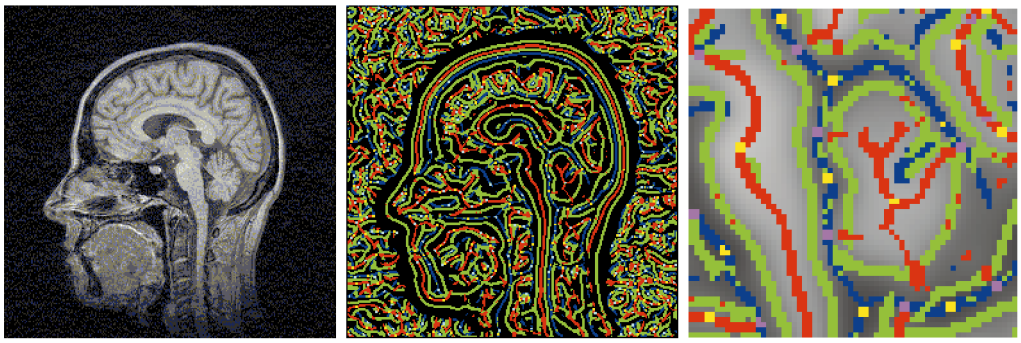

(a) (b) (c)

Fig. 5. (a) An MRI 256×256 sagittal image of a human head. (b) Complete set of 2D positive ridges (red) and negative ridges (blue), edges (green) and singular points (extrema: yellow, saddle points: purple). The calculations are done for a spatial scale of two pixels. (b) A 64×64 fragment of the original image is superimposed with the corresponding RCPS.

TABLE 3
The Possible Point-Sets for Three-Dimensional Signals

m_+ / m_-	0	1	2	3
0	regular	negative surface	negative string	minimum
1	positive surface	saddle string	saddle point (1)	x
2	positive string	saddle point (2)	x	x
3	maximum	x	x	x

An "x" stands for an impossible configuration.

two-dimensional ridge and that the string of maxima is the local maximum of the blob at that scale.

In Fig. 6d, we have depicted the sets $R^{0,1}$, positive surface, $R^{1,0}$, negative surface, $R^{0,2}$, string of maxima, and $R^{2,0}$, string of minima of the natural Laplacian of the blob. The natural Laplacian is the operator $\sigma^2\Delta$. The middle surface has become a negative surface in comparison to Fig. 6b because the main lobe of the second derivative of the

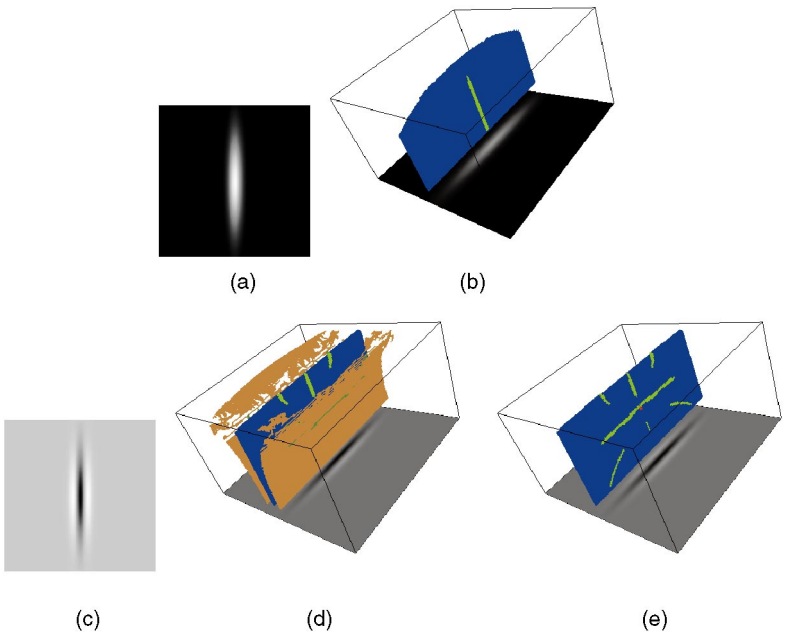

(a) (b) (c) (d) (e)

Fig. 6. (a) A two-dimensional anisotropic Gaussian blob with $\sigma_x = 5.0$ and $\sigma_y = 35.0$ pixels. (b) The positive surface (blue) and the string of maxima (green) of the blob in scale space. At the bottom of the box, we have shown the blob again. The scale runs exponentially in 64 steps from 1.0 to 20.0 pixels upward in the figure box. The image was 128 pixels square. (c) The natural Laplacian of the blob at a scale of 1.0 pixel. (d) Positive surfaces (brown) of the natural Laplacian of the blob in scale, negative surface (blue) of the natural Laplacian of the blob in scale, strings of maxima (dark green, on the positive surface), and strings of minima (light green, on the negative surface). (e) Negative surface (blue) of the natural Laplacian of the blob in scale, strings of minima (light green), and a local minimum (red).

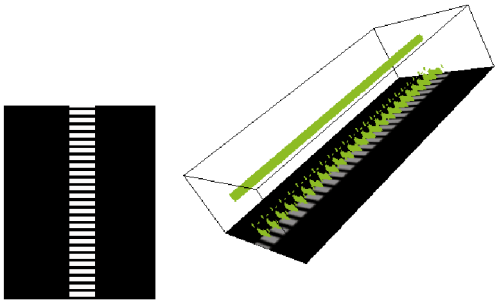

(a) (b)

Fig. 7. (a) An image of 64×128 pixels with bars of 11×3 pixels. The bars are separated by two pixels. (b) The scale space strings of the natural Laplacian of (a). The scale runs exponentially from 1.0 to 10.0 pixels in 32 steps.

Gaussian is negative. The positive surfaces are due to the second derivative. The strings of maxima are subsets of the positive surface, cf. (18).

For clarity, we have shown, in Fig. 6e again, the negative surface and the strings of minima and added the set $R^{3,0}$, a local minimum, which was invisible in Fig. 6d because of the positive surfaces. As with the positive strings, the strings of minima are subsets of the negative surface, whereas the local minimum is a subset of the negative strings. Going from small scales to large scales, we see two strings start at the endpoints of the Laplacian of the blob. For increasing scales, they start to converge to the middle. In the same scale range, we see a string at the middle which is oriented in the scale direction. Then, we have a scale range in which no strings are found because the scale space structures interfere with each other and it is no longer possible to define a local coordinate frame based on the Hessian. For still larger scales, we find a primarily horizontal string, marking the optimal scale at which the negative part of the Laplacian of the blob can be detected. On the horizontal string, we find, in red, a local minimum. For the larger scales, three strings start to disperse for increasing scale, the middle one being vertical. If we extrapolate the small scale vertical string upward, i.e., to larger scales, and the large scale vertical string downward, they connect and cross the horizontal string in the local minimum, which is the optimal minimum with respect to scale.

As a final set of examples, we show how we can introduce model information by choosing a particular local vector frame instead of the local Hessian frame field from the general Definition 4. We will concentrate on the detection of elongated structures in two-dimensional images.

First, we show an example of a synthetic two-dimensional image of horizontal bars, see Fig. 7. Clearly, this image has two optimal scales at which elongated structures can be detected. At small scales, we perceive the horizontal bars separately, but, at larger scales, they will be grouped into a vertical line. If we would use the natural Laplacian for building a scaling representation of the image, we could compute the one-dimensional RCPS for detecting these two types of structures, but, in such a construction, we would also detect vertical strings representing the scale evolution of the local extrema and saddle points of the two-dimensional image. To suppress the vertical strings, we have selected the two-dimensional frame field $h(x)$ from the general Definition 4 with one of the vectors fixed in the direction of increasing scale. The other frame vector is determined by the largest absolute eigenvalue of the Hessian in the xy-plane. We refer to these strings as *scale space strings*. Clamping one of the frame vectors in the direction of the scale parameter is a natural choice for detecting elongated structures of two-dimensional images in scale space. It is dictated by the interpretation of the final result as elongated structures in the original image *lifted* to a certain scale. This scale we can interpret as the *optimal scale* of response for the corresponding structure.

Fig. 7a shows the scale space strings of the right image. For small scales (bottom of the box), we find the horizontal bars whereas, for larger scales, they are grouped on a vertical line.

The following example is a two-dimensional fundus reflection image from a scanning laser ophthalmoscope, see Fig. 8, in which we want to detect the vessels of the retina at their optimal scale, i.e., we want to detect two-dimensional elongated structures at their optimal scale. To this end, we have segmented out the scale space strings of the natural Laplacian, as discussed in the previous example. Fig. 8a shows in green the scale space strings which detect the elongated structures at their optimal scale in scale space.

Another way for detecting elongated structures in two-dimensional images can be provided by local orientation analysis. With any gray-scale 2D image, we can associate an 3D orientation bundle given as:

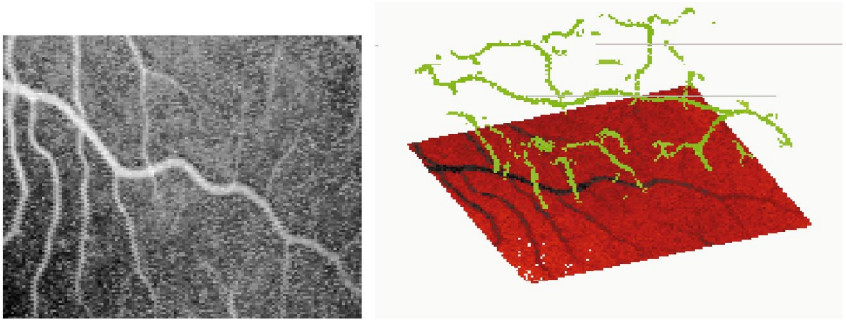

(a) (b)

Fig. 8. (a) Vessel structure of the retina. (b) Scale space strings (green) of the natural Laplacian of (a). We fixed one vector of the local frame field in the direction of increasing scale.

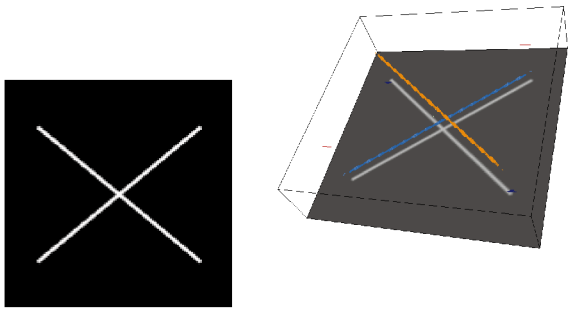

(a) (b)

Fig. 9. (a) Simulated 128×128 pixels image representing two crossing lines. (b) Orientation space strings obtained as RCPS derived from the 2D frame field, where one vector always points vertically in the θ direction. The other vector is $(-\sin\theta, \cos\theta, 0)$, i.e., it is perpendicular to the local orientation of the filter. The local angle (vertical axis) is color-coded (0 is dark blue, π is red) for better rendering effect.

$$F(x,y,\theta) = \int dx'dy'\Phi(x-x', y-y', \theta)L(x', y'), \qquad (21)$$

where $\Phi(x,y,\theta)$ is any orientation filter. In such a representation, the bundle can be regarded as a 3D signal in the space (x,y,θ).

A natural choice for the frame field in this case is a 2D vector subframe in which one of the vectors is always in the direction of angular changes, i.e., in the vertical direction, and the second vector points in the direction perpendicular to the angle at the point (x,y,θ), i.e., $(-\sin\theta, \cos\theta, 0)$, since maximal response for an elongated structure is to be expected *along* the direction of the orientation filter.

In the following examples, we have chosen as the orientation filter an anisotropic Gaussian kernel with a scale of 1.0 pixel along the short axis and 8.0 pixels along the long axis. In Fig. 9, we depict the positive strings relative to the above-defined two-dimensional vector frame for an image of two crossing lines. The angle runs from 0 to π in 32 steps.

We clearly see that the two lines "unsplit" in the orientation bundle. They cross at the same space position, but at different angles. We have only computed the bundle for $\theta \in [0, \pi)$ because of the $\theta \rightarrow \theta + \pi$ symmetry of the filter.

Finally, in Fig. 10, we present the same analysis as in Fig. 10 but for another fundus reflection image. In Fig. 10a, we show all the positive strings that were computed. In Fig. 10b, we show the 22 longest strings. Both images clearly show the unsplitting in orientation space of crossing structures.

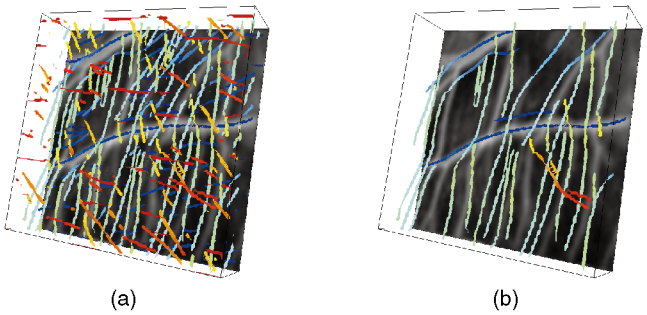

(a) (b)

Fig. 10. Orientation space strings for a retinal image. (a) Depicts all computed positive strings and (b) the 22 longest. The vector frame is chosen as in the computation presented in Fig. 9.

5 Applicability and Validation of the Method

The introduced method is based on the *constructive Definition 4* of the RCPS and, therefore, there is no need for intrinsic validation of the scheme. Any data point that obeys the definitive condition belongs to the set and vice versa. Different RCPS definitions can, of course, lead to different point-sets, but each one of the latter will be consistent with its own definition.

However, an important validation question arises in relation to the *interpretation* of the RCPS of various signature as specific image properties with perceptual significance. Such a correspondence will justify (or deny) the application of these mathematical constructions in real image analysis.

RCPS represent, in general, subdimensional structures in images such as one-dimensional string-like structures (catheters, blood vessels, etc.) or two-dimensional surface types of structures (edges, fault surfaces in seismic data, etc.). If a given image feature can be *modeled or approximated* with such structures, then the RCPS method can applied successfully.

We show an example in Fig. 11 from a real clinical application where a dense network of blood-vessels in optical image of human retina has to be segmented before laser treatment. We simplify the problem by first modeling the blood-vessels as one-dimensional structures and approximate them with their center luminance line. In a later stage (not reported here), we attach a width to these elongated structures. It is easy to see from the result in Fig. 11b that the sensitivity of the system of ridges when used to represent the center lines of the blood vessels is nearly 100 percent. At the same time, the specificity of the method is low because not all of the ridges, in fact, very few of them, represent actual blood vessels. The system of ridges serves as a superset from which one has to recognize and select those ridges corresponding to segments of blood vessels. The description of the methods used to do this goes beyond the scope of the present paper. After applying a neural network classifier, we have obtained the final result in Fig. 11c.

To generalize, the proposed method of building the RCPS in a given application can be used successfully only in combination with preprocessing stages (such as image regularization) and postprocessing filtering or classification. Therefore, it is difficult to assess the performance of our technique as a standalone method. The above external validation can distinguish between different critical point-set definitions and their relevance for image processing tasks. We compare our method to the definition of ridges used by Eberly et al. [4], [3] and, recently, by Miller [15] and Keller [11]. In the later approaches, when applied to 2D images, positive ridges are defined as the point-set where the gradient vector is orthogonal to the principal direction of the Hessian corresponding to the lowest negative eigenvalue. We have adapted our own computational method to calculate ridges according to both definitions. The results of the comparison are shown in Fig. 12. We see that our method produces a smaller point-set, but, in this application, there is no loss of

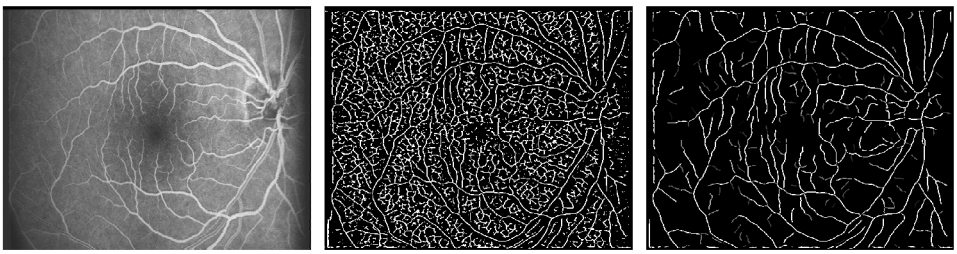

(a) (b) (c)

Fig. 11. (a) Optical fluorescence image of the fundus of human retina. (b) Full system of positive ridges computed at regularization scale of one pixel. (c) The point-set of ridges is classified with feedforward neural classifier. The result shows the center lines of the detected blood vessels.

sensitivity as all the extra ridges detected by the second method do not correspond to blood vessels. We conclude, therefore, that our method has increased the specificity for the blood vessels detection task without loss of sensitivity.

6 Conclusions

In this paper, we proposed a constructive definition of relative critical sets in images of any number of spatial dimensions. The definition is very flexible because it associates critical sets to an arbitrary chosen local vector frame field. Depending on the visual task, different model structures can be identified with the relative critical sets. As a consequence, our construction can be purely intrinsic (defined only by the image structures) or it can involve externally specified frames. The last situation may be useful for involving additional model information. In this paper, we demonstrated the examples of one of the most-popular intrinsic cases: the set of topological ridges.

The relative critical sets are, in general, connected submanifolds. Therefore, our technique indeed provides a method for *perceptual grouping* achieved with only *local* measurements. In a sense, such a technique can be viewed as a particular extension of the threshold techniques where the connected entities are the level surfaces (or lines in 2D).

The grouping properties of the system of ridges were demonstrated in the paper in the application for optimal scale selection of a multiscale connected object (see Fig. 6). The method also provides a *linkage* from the scale-space structure down to the original image space. We refer to those applications as to *topological deep-structure analysis*.

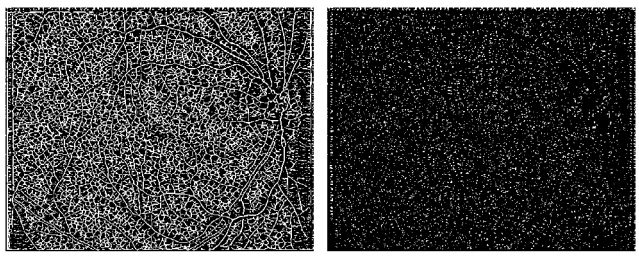

(a) (b)

Fig. 12. (a) Full system of positive ridges computed as RCPS, where the gradient is orthogonal to the lowest negative eigenvector of the Hessian. The input image and all the parameters are the same as in Fig. 11. (b) The difference between the ridges of (a) and the system of ridges computed with our method (cf. Fig. 11b).

In the above examples, the externally specified vector frames incorporate model information. One example concerned scale space grouping, see Figs. 7 and 8. Another example shown is grouping of elongated structures in an orientation bundle representation of 2D images (see Figs. 9 and 10).

As already discussed in Section 5, the major criteria for applying this technique is the correspondence of the RCPS to *essential image features*. The important features of the image are those that determine the context content of the image in large scale. Therefore, further processing is required to select only those subsets of the RCPS that are relevant for the larger scale context. For the case of blood vessels detection, the result in Fig. 11 is obtained by first decomposing the point-set of positive ridges into smooth, convex subsets and, subsequently, applying a feedforward neural network classification on these subsets. In more complicated situations, large scale grouping techniques may be needed to select, in a context-dependent way, the relevant subsets of RCPS.

Appendix

Numerical Implementation

In this section, we discuss only the computation algorithm of formulas (11) and (12). According to the previous sections, the integral has to be calculated on a surface lying in a linear subspace and taken close around a given test point. The computation of the vectors defining this subspace (when necessary) depends on the application and will not be presented here. In the case of ridges, for example, the principle directions of the Hessian can be obtained by any diagonalization procedure. We assume in what follows that the linear space is defined in every image point by a given orthonormal system of vectors h^i_α, $i = 1, \ldots, D$, $\alpha = 1, \ldots, D_K$.

To compute (11), we will use its topological property that it can be defined by integration of (5) on *any* surface surrounding the test point P with vector coordinates x_P. Therefore, we can select, for a border, a D_K-dimensional *cube*, the ribs of which are parallel to h^i_α. The surface is formed by $2D_K$, $D_K - 1$-dimensional cubes, parallel in pairs, which we denote as S^+_A, S^-_A, $A = 1, \ldots, D_K$. If $D_K = 2$, for example, $S^\pm_A, A = 1, 2$ are just line segments; if $D_K = 3$, then $S^\pm_A, A = 1, 2, 3$ are the six walls of the cube, etc. Next, we *parameterize* the integration points on each of the cubes $S^\pm_A$ as:

$$x_A^{\pm}(s_1,\ldots,s_{D_K-1}) = x_P \pm \frac{R}{2}h_A + \sum_a^{D_K-1}\left(s_a\frac{R}{N}-\frac{R}{2}\right)h_{t(A,a)}, \tag{22}$$

where the explicit D-dimensional index i is omitted. The real constant R measures the size of the neighborhood around the point P and represents our spatial precision. The integer constant N represents the number of integration points along each direction of the cube border. Finally, the function $t(A,a)$ gives the ath element from the set $[1,\ldots,D_K]-[A]$ or, in other words, $t(A,a)=a$ when $a<A$ and $t(A,a)=a+1$ when $a\geq A$. Surface coordinates $s_a, a=1,\ldots,D_K-1$ in (22) take integer values $1,\ldots,N$.

We can compute the projected gradient vector in these points according to (10):

$$L^{\pm}_{\alpha,A}(s_1,\ldots,s_{D_K-1}) \equiv \sum_i h^i_\alpha(x)L_i(x)\big|_{x=x_A^{\pm}(s_1,\ldots,s_{D_K-1})}. \tag{23}$$

For the examples in this paper, we have used a simple multidimensional interpolation algorithm of first order to calculate the gradient values with subpixel precision in (23). Because of the topological nature of the quantity (11) any interpolation algorithm will give the same result.

Substituting the differentials in (5) with finite differences on the borders $S_A^{\pm}$ and the integration in (11), with summation over the indices $s_1,\ldots,s_{D_K-1}$, we obtain the following expression for the discrete computation of the topological number:

$$\begin{aligned}\nu_K(x_P) = &\\ &\frac{1}{N^{D_K-1}}\sum_A^{D_K}\sum_{\sigma=+1,1}\sigma\sum_{\alpha_1,\ldots,\alpha_{D_K}}\epsilon^{\alpha_1,\ldots,\alpha_{D_K}}\\ &\sum_{s_1,\ldots,s_{D_K-1}} L^{\sigma}_{\alpha_1,A}(s_1,\ldots,s_{D_K-1})L^{\sigma}_{\alpha_2,A}(s_1+1,\ldots,s_{D_K-1})\\ &L^{\sigma}_{\alpha_3,A}(s_1,s_2+1,\ldots,s_{D_K-1})\cdots L^{\sigma}_{\alpha_{D_K},A}(s_1,\ldots,s_{D_K-1}+1).\end{aligned} \tag{24}$$

In the above formula, the antisymmetry of the tensor ϵ has been used to exclude components symmetric in the indexes α.

ACKNOWLEDGMENTS

The authors would like to thank Tos Berendschot for providing the fundus reflection images and Alejandro Frangi for helping with the three-dimensional rendering.

This work was carried out in the framework of the NWO research project STW/4496.

REFERENCES

[1] W.M. Boothby, *An Introduction to Differential Geometry and Riemannian Geometry.* New York: Academic Press, 1975.
[2] J. Damon, "Generic Structure of Two-Dimensional Images under Gaussian Blurring," *SIAM J. Applied Math.,* vol. 59, pp. 97-138, 1998.
[3] D. Eberly, *Ridges in Image and Data Analysis.* Dordrecht: Kluwer Academic, 1996.
[4] D. Eberly, R. Gardner, B. Morse, S. Pizer, and C. Scharlach, "Ridges for Image Analysis," *J. Math. Imaging and Vision,* vol. 4, pp. 351-371, 1994.
[5] T. Eguchi, P. Gilkey, and J. Hanson, "Gravitation, Gauge Theories and Differential Geometry," *Physics Reports,* vol. 66, no. 2, pp. 213-393, 1980.
[6] P. Johansen, "On the Classification of Toppoints in Scale-Space," *J. Math. Imaging and Vision,* vol. 4, no. 1, pp. 57-68, 1994.
[7] S.N. Kalitzin, "Topological Numbers and Singularities in Scalar Images Scale-Space Evolution Properties," *Gaussian Scale-Space Theory,* J. Sporring, M. Nielsen, L. Florack, and P. Johansen, eds., pp. 181-189, Dordrecht: Kluwer Academic, 1997.
[8] S.N. Kalitzin, B.M. ter Haar Romeny, A.H. Salden, P.F.M. Nacken, and M.A. Viergever, "Topological Numbers and Singularities in Scalar Images Scale-Space Evolution Properties," *J. Math. Imaging and Vision,* vol. 9, no. 3, pp. 253-269, 1998.
[9] S.N. Kalitzin, B.M. ter Haar Romeny, and M.A. Viergever, "On Topological Deep-Structure Segmentation," *Proc. Int'l Conf. Image Processing,* pp. 863-866, Oct. 1997.
[10] M. Kass, A. Witkin, and D. Terzopoulos, "Snakes: Active Contour Models," *Proc. IEEE First Int'l Computer Vision Conf.,* 1987.
[11] R. Keller, "Generic Transistions of Relative Critical Sets in Parametrized Families with Application to Image Analysis," PhD thesis, Dept. of Math., Univ. of North Carolina, Chapel Hill, 1999.
[12] J.J. Koenderink, "The Structure of Images," *Biological Cybernetics,* vol. 50, pp. 363-370, 1984.
[13] T. Lindeberg, "Scale-Space Behaviour of Local Extrema and Blobs," *J. Math. Imaging and Vision,* vol. 1, no. 1, pp. 65-99, 1992.
[14] T. Lindeberg, *Scale-Space Theory in Computer Vision.* Dordrecht: Kluwer Academic, 1994.
[15] J. Miller, "Relative Critical Sets in $\mathbf{R}^n$ and Application to Image Analysis," PhD thesis, Dept. of Math., Univ. of North Carolina, Chapel Hill, 1998.
[16] M. Morse and S.S. Cairns, *Critical Point Theory in Global Analysis and Differential Topology.* New York: Academic Press, 1969.
[17] M. Nakahara, *Geometry, Topology, and Physics.* New York: Adam Hilger, 1989.
[18] O.F. Olsen, "Multi-Scale Watershed Segmentation," *Gaussian Scale-Space Theory,* J. Sporring, M. Nielsen, L. Florack, and P. Johansen, eds., Dordrecht: Kluwer Academic, 1997.

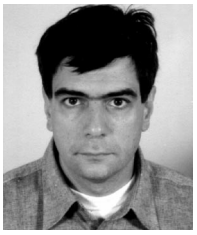

Stiliyan N. Kalitzin graduated with a degree in nuclear physics in 1981 from the University of Sofia, Bulgaria. Working as a research associate in academic institutes, he received, in 1988, the PhD degree in theoretical physics, where he made contributions to the foundation and the development of the harmonic superspace theory. In 1990, he was enrolled as a post-doctoral student at the University of Utrecht, Institute of Theoretical Physics, where he continued his work on supersymmetry and supergravity and also got involved in research on cellular automata, neural networks, and related topics. In 1992, he joined the Visual Systems Analysis Group at the University Hospital in Amsterdam, where he has contributed to the development and analysis of biological neural network models of the human vision. From 1996 to 1999, he worked at the Image Sciences Institute at University Medical Center in Utrecht in the area of multiscale image analysis, orientation filters, topological analysis of images, and perceptual grouping. Since 1999, he has been with the Dutch Epilepsy Clinics Foundation where he heads the Medical Physics Department. His current research interests are in the fields of nonlinear system dynamics, signal processing, seizure prediction, and large scale neural network modeling of epileptic brain activity.

Joes Staal received the MSc degree in applied physics from Delft University of Technology in 1995. In 1996, he began working on a PhD degree in the Department of Geodesy of the Delft University of Technology on the subject of multiresolution boundary element methods. In 1997, he left this position for a PhD at the Image Sciences Institute, Utrecht University. He worked with Stiliyan Kalitzin on the subject of multiscale image analysis, topological image analysis, and perceptual grouping. His research interests are in multiscale analysis, (continuous) wavelet transforms, pattern recognition, and perceptual grouping.

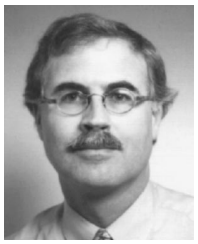

Bart M. ter Haar Romeny received the MSc degree in applied physics from Delft University of Technology in 1978 and the PhD degree in neuromuscular nonlinearities from Utrecht University in 1983. After being the principal physicist of the Utrecht University Hospital Radiology Department, he joined the Department of Medical Imaging at Utrecht University as associate professor in 1989. He is a permanent staff member of the Image Sciences Institute of Utrecht University and the University Hospital Utrecht and chairman of the Dutch Biophysical Society. His interests are mathematical aspects of visual perception, in particular, linear and nonlinear scale-space theory, computer vision applications, and all aspects of medical imaging. He is the author of numerous papers and book chapters on these issues, has edited books on nonlinear diffusion theory and scale-space theory in computer vision, and, initiated a number of international collaborations on those subjects. He is an active teacher in international courses, a senior member of the IEEE, and an IEEE Chapter Tutorial Speaker.

Max A. Viergever received the MSc degree in applied mathematics in 1972 and the DSc degree with a thesis on cochlear mechanics in 1980, both from Delft University of Technology. From 1972 to 1988, he was an assistant/associate professor of applied mathematics at Delft University of Technology. Since 1988, he has been a professor and the head of the Department of Medical Imaging at Utrecht University. Since 1996, he has been an adjunct professor of computer science at Utrecht University, since 1996 he has been the scientific director of the Image Sciences Institute of the University Medical Center Utrecht, and, as of 1998, director of the Graduate School of Biomedical Image Sciences (ImagO). He has coauthored more than 300 refereed scientific articles (abstracts excluded) on biophysics and medical image processing, has been the guest editor of seven journal issues, and has been a coauthor/editor of 14 books. His research interests comprise all aspects of computer vision and medical imaging. He is a board member of IAPR, IPMI, and MICCAI, he is editor of the book series *Computational Imaging and Vision* (Kluwer Academic Publishers), associate editor-in-chief of the *IEEE Transactions on Medical Imaging*, editor of the *Journal of Mathematical Imaging and Vision*, and participates on the editorial boards of five more international journals.